Article

Structure, Vibrational Analysis, and Insights into Host–Guest Interactions in As-Synthesized Pure Silica ITQ-12 Zeolite by Periodic B3LYP Calculations

Claudio Marcelo Zicovich-Wilson, Mara Luisa San-Romn, Miguel Angel Camblor, Fabien Pascale, and Jos Sergio Durand-Niconoff

J. Am. Chem. Soc., **2007**, 129 (37), 11512-11523• DOI: 10.1021/ja0730361 • Publication Date (Web): 25 August 2007

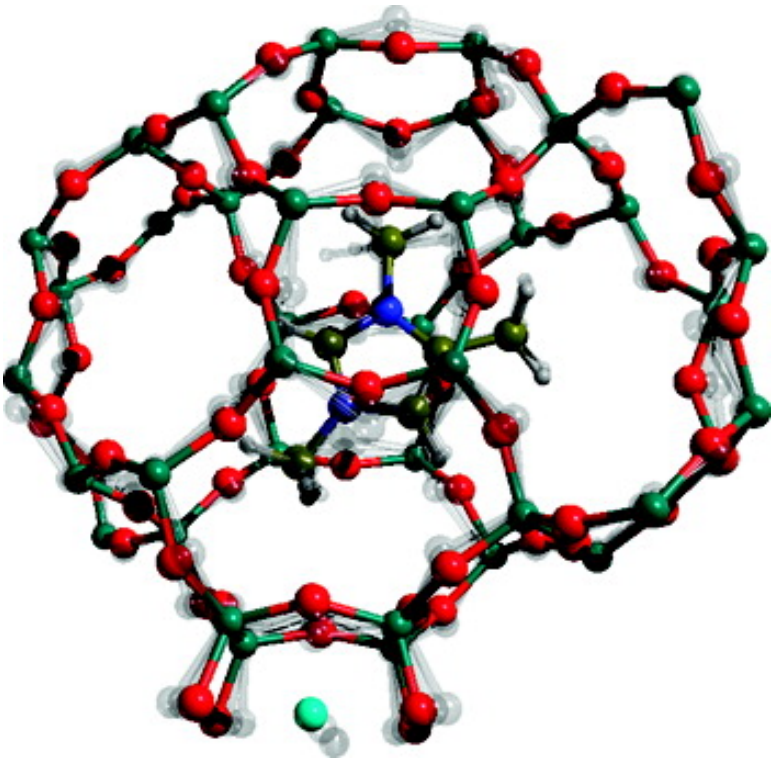

J|A|C|S
ARTICLES
Published on Web 08/25/2007

Structure, Vibrational Analysis, and Insights into Host−Guest Interactions in As-Synthesized Pure Silica ITQ-12 Zeolite by Periodic B3LYP Calculations

Claudio Marcelo Zicovich-Wilson,*,† María Luisa San-Román,‡ Miguel Angel Camblor,§ Fabien Pascale,|| and José Sergio Durand-Niconoff†,⊥

Contribution from the Facultad de Ciencias, Universidad Autnóma del Estado de Morelos, Av. Universidad 1001, Col. Chamilpa, 62209 Cuernavaca (Morelos), Mexico, Centro Investigaciones Químcas, Universidad Autnóma del Estado de Morelos, Av. Universidad 1001, Col. Chamilpa, 62209 Cuernavaca (Morelos), Mexico, Instituto de Ciencia de Materiales de Madrid (CSIC), Departamento de Materiales Porosos y Compuestos de Intercalación C/ Sor Juana Inés de la Cruz 3 Campus Cantoblanco 28049 Madrid, Spain, and Laboratoire de Cristallographie et Modélisation des Matériaux Minéraux et Biologiques, Vandoeuvre-lès-Nancy, Cedex 05, 54506 France

Received April 30, 2007; E-mail: claudio@servm.fc.uaem.mx

Abstract: As-made and calcined ITQ-12 zeolites are structurally characterized by means of the analysis of their vibrational modes. The experimental IR spectra made on high crystalline samples are compared with accurate B3LYP periodic calculations performed with the CRYSTAL06 code. The fair agreement between both sets of data allows us to make a reliable assignment of the IR modes. Thanks to the detailed information provided by the theoretical calculations, the analysis of the IR intensities, the Born dynamic charges, and the whole set of vibrational frequencies at Γ-point shed light on several aspects of the host−guest interaction, structure−direction issues, including the role of fluoride anions in allowing the crystallization of silica structures with strained double-four rings, and the role played by the framework flexibility.

1. Introduction

Pure silica zeolites synthesized through the fluoride route combine, after calcination, the microporous nature of zeolites with a strict hydrophobic character provided by the absence of net charges in their defect-free network of four-connected $SiO_{4/2}$ tetrahedra.[1] In addition to their interest in separation processes, the synthesis of this type of materials presents peculiar characteristics concerning host−guest interactions and structure-directing effects, which are distinctly different from those observed through the more classical hydroxide synthesis route. The materials prepared by the fluoride route contain both fluoride anions and organic cations occluded in nearly equimolar amounts.[1] Fluoride typically resides within small cavities of the SiO_2 framework at a relatively large distance of the positively charged cation, from which it is separated by silica walls.[2] Depending on the material and temperature, fluoride anions may interact with Si atoms in a variety of ways,[3] resulting in either (a) well-defined Si−F bonds in steady pentacoordinated $[SiO_{4/2}F]^-$ units, (b) dynamic situations with F^- jumping to make transient Si−F bonds to different Si atoms, or (c) encapsulated fluoride with no empirical evidence of Si−F bonding (as it happens when fluoride is occluded in a double four ring unit, D4R). By contrast, pure and high silica zeolites crystallized by the hydroxide route do not occlude hydroxide anions: the charge balance of positively charged organic cations is attained by the presence of silanolate Si−O^- groups, which are involved in strong hydrogen bonds with nearby Si−OH silanols, resulting in a high concentration of connectivity defects[4] and possibly allowing a closer interaction between both charged species. Perhaps related to these differences in host−guest interactions, structure-directing effects appear to be quite dissimilar in both synthesis routes, as inferred by the fact that certain SiO_2 materials, which readily crystallize by the fluoride route, have never been obtained in the absence of this anion.[2] Among these, materials containing D4R units are prominent: octadecasil (structure type code[5] AST),[6] polymorph C of the Beta family (BEC),[7] ITQ-7 (ISV),[8] ITQ-12 (ITW),[9] and ITQ-13 (ITH)[10] have so far avoided their synthesis as SiO_2 materials by the hydroxide

† Facultad de Ciencias, Universidad Autnóma del Estado de Morelos.
‡ Centro Investigaciones Químcas, Universidad Autnóma del Estado de Morelos.
§ Instituto de Ciencia de Materiales de Madrid (CSIC).
|| Vandoeuvre-lès-Nancy.
⊥ On leave from Universidad Veracruzana, Xalapa, Mexico.

(1) Caullet, P.; Paillaud, J. L.; Simon-Masseron, A.; Soulard, M.; Patarin, J. *C. R. Chim.* **2005**, *8*, 245−266.
(2) Villaescusa, L. A.; Camblor, M. A. *Recent Res. Dev. Chem.* **2003**, *1*, 93−141.
(3) Koller, H.; Wölker, A.; Villaescusa, L.; Díaz-Cabañas, M. J.; Valencia, S.; Camblor, M. A. *J. Am. Chem. Soc.* **1999**, *121*, 3368−3376.
(4) Koller, H.; Lobo, R. F.; Burkett, S. L.; Davis, M. E. *J. Phys. Chem.* **1995**, *99*, 12588−12596.
(5) Meier, W. M.; Olson, D. H. *Atlas of Zeolite Structures*; Butterworth: London, 1996.
(6) Caullet, P.; Guth, J. L.; Hazm, J.; Lamblin, J. M.; Gies, H. *Eur. J. Solid State Inorg. Chem.* **1991**, *28*, 345.
(7) Liu, Z.; Ohsuna, T.; Terasaki, O.; Camblor, M. A.; Díaz-Cabañas, M. J.; Hiraga, K. *J. Am. Chem. Soc.* **2001**, *123*, 5370−5371.
(8) Villaescusa, L. A.; Barrett, P. A.; Camblor, M. A. *Angew. Chem., Int. Ed.* **1999**, *38*, 1997−2000.

10.1021/ja0730361 CCC: $37.00

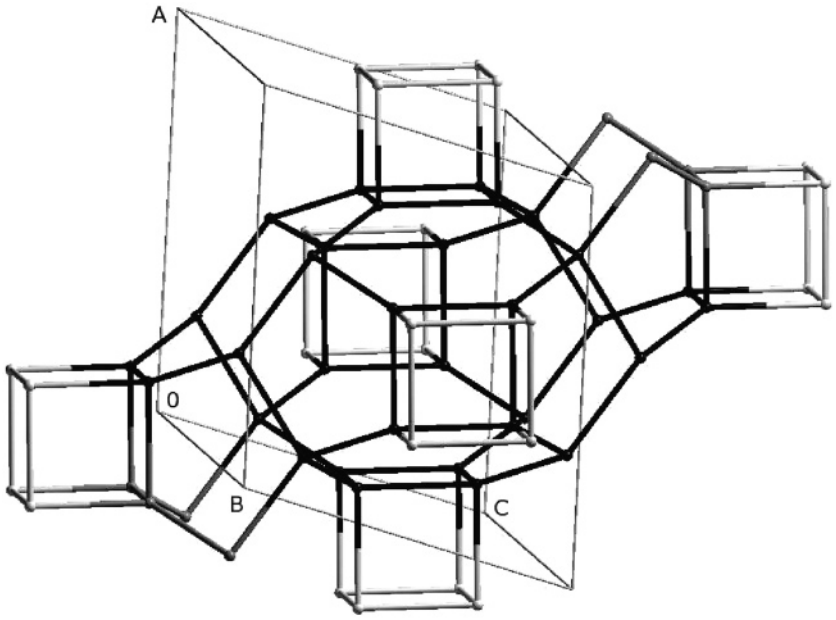

Figure 1. Schematic representation of the ITQ-12 cages. The black part corresponds to the obloid [$4^5 5^4 6^4 8^4$] cage. The larger [$4^6 5^8 6^4 8^4$] (8R-CI) unit is formed with the addition of the gray sticks, and the light gray part shows how the neighboring 4^6 (D4R) units are connected to the cage. The conventional cell is shown in thin lines.

route. The apparent ability of fluoride to mediate the crystallization of structures with D4R units has prompted the idea that the fluoride anion has a structure-directing effect of its own, which has to be considered in addition to the effect exerted by the organic cation.[1,2]

The investigation of host−guest interactions and structure-directing effects in silica zeolites synthesized by the fluoride route is, thus, well merited. Complementing the empirical methods that probe short range order in solids, it is now becoming possible, though costly, to face the challenge of investigating crystalline materials by accurate theoretical calculations, allowed by the increasing computational power and the efforts made to implement high level theory calculations which include periodicity.[11] Such calculations may reveal structural details not accessible by conventional diffraction techniques that average the structure within the time and space scale of the experiment. Here we present our investigation of as-made and calcined ITQ-12, a pure silica zeolite with a large potential in important applications and which contains D4R units in its structure.

The small-pore ITQ-12 zeolite[9,12] has recently attracted great interest owing to its efficient molecular sieving property in the separation of propene from propene/propane mixtures.[12,13] The absence of defects that could give rise to catalytic sites avoids pore blockage by acid-catalyzed polymerization, while adsorption is not distorted by the presence of humidity thanks to the hydrophobicity of the siliceous material. The material shows a peculiar temperature-dependent adsorption behavior, with propane adsorption rapidly falling as the temperature rises, while propene adsorption decreases only moderately.[13] The resulting selectivity in the separation process is essentially 100% at 80 °C, which makes ITQ-12 a very promising adsorbent for a new, more efficient pressure swing adsorption industrial process. This is an important and large-volume operation in the chemical and petrochemical industry which is currently achieved using a very energy-intensive fractional distillation procedure.

The structural determination of the as-made and calcined pure silica ITQ-12, synthesized through the F-route with 1,3,4-trimethylimidazolium (TMI^+) as a structure-directing agent (SDA), has been the subject of a previous work using synchrotron powder diffraction data.[14] According to it, [$Si_{24}O_{48}$]-ITQ-12, structure code ITW, is a monoclinic (*C*1*m*1) eight-ring pure silica zeolite that contains obloid [$4^5 5^4 6^4 8^4$] cages having an ~3.9 Å × 9.6 Å × 8.5 Å internal size. While consideration of these cavities is essential to account for diffusion processes and host−guest interactions in the zeolite, from the topological point of view it is probably more appropriate to consider a larger unit [$4^6 5^8 6^4 8^4$] which represents the 8R channel intersection (8R-CI) and includes the obloid cage together with two additional subunits,[5] in the manner depicted in Figure 1.

Each of those large units is shared by six neighboring double four-ring (D4R) units, and all of them are connected to each other through the five-, six-, and eight-ring units, forming a 3-D topology (see Figure 1). As concerns the eight-ring cage openings, they can be classified into two different types. Those of dimensions 2.4 Å × 5.3 Å appear to be too narrow to allow passages of even the smallest hydrocarbon. The other type of eight-ring cage possesses a 3.8 Å × 4.1 Å opening, which is close to the cross sections of propene and propane molecules.[12] It is worth noting that in the as-made material the fluoride anion is located close to the center of the D4R unit, while the TMI^+ occupies the larger obloid cage with the planar ring lying on

(9) Boix, T.; Puche, M.; Camblor, M. A.; Corma, A. U.S. Patent 6,471,939, 2002.
(10) Boix, T.; Puche, M.; Camblor, M. A.; Corma, A. U.S. Patent 6,471,941, 2002.
(11) *Quantum-Mechanical ab initio calculation of the properties of crystalline materials*; Pisani, C., Ed.; Springer: Berlin, Heildelberg, 1996; Vol. 67.
(12) Barrett, P. A.; Boix, T.; Puche, M.; Olson, D. H.; Jordan, E.; Koller, H.; Camblor, M. A. *Chem. Commun*. **2003**, 2114−2115.
(13) Olson, D. H.; Yang, X.; Camblor, M. A. *J. Phys. Chem. B* **2004**, *108*, 11044−11048.
(14) Yang, X.; Camblor, M. A.; Lee, Y.; Liu, H.; Olson, D. H. *J. Am. Chem. Soc.* **2004**, *126*, 10403−10409.

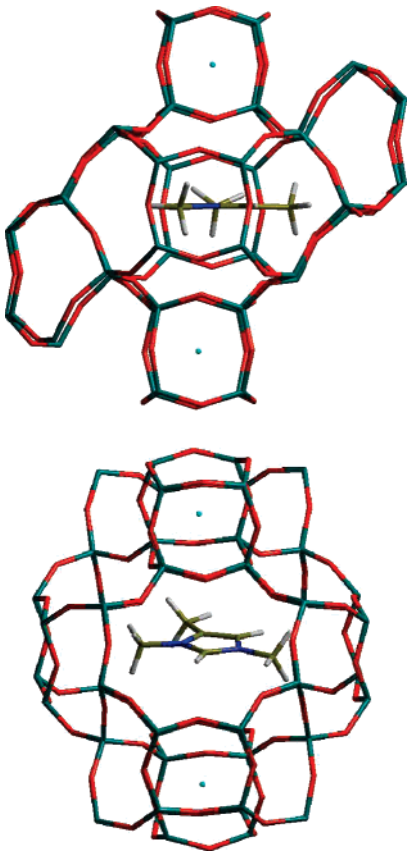

Figure 2. Two views of the TMI^+ and F^- ions occluded into the ITQ-12 cavities, as determined in this work.

the equatorial plane of the cage (see Figure 2). Both the organic cation and the fluoride anion are considered essential for the synthesis of the pure silica material, for which a cooperative structure-directing effect has been invoked.[2,14]

The aim of the present work is to provide a more detailed description of the structural characteristics of pure silica zeolites with D4R framework units synthesized through the fluoride route, taking ITQ-12 as a representative (as-made and calcined). The main reasons for this choice are the extremely low amount of defects in the synthesized samples, which allow a thorough comparison between theoretical and experimental vibrational spectra, and the relatively low number of atoms per cell, which makes high level periodic calculations affordable with current computational resources. To this purpose, an analysis of the vibrational modes of the materials is performed at the hybrid DFT level of theory considering the periodic approach as implemented in the CRYSTAL06 code.[15,16]

This methodology has been proved to be extremely accurate in the investigation of the vibrational spectra of several oxides,[17−23] and as far as we know, it has never been adopted for the study of the lattice vibration of zeolites, either pure or with occluded species. As a matter of fact, previous works have been essentially devoted to the study of zeolite lattice dynamics by means of low level forcefield methods,[24−28] and only recently, a few studies appeared in which periodic DFT methods are considered to simulate parts of the zeolitic phonon spectra, to study both the framework vibrations[29−32] and host−guest interactions.[33−40]

Thanks to the excellent agreement between the simulated and experimental IR and RAMAN spectra, which results from both the quite good accuracy of the computational method and the high crystallinity of the samples, the modes can be characterized in detail and classified according to the structural units involved in their motions. The dipole moment change, which is closely related to the IR absorption intensity, is also considered in the analysis so as to give some insight on the nature of the host−guest interactions.

2. Experimental Section

2.1. Synthesis of ITQ-12. Pure silica ITQ-12 was synthesized by slight variations of previously reported procedures,[12] using TMI^+ hydroxide and hydrofluoric acid. The organic cation was synthesized by methylation at both N atoms of 4(5)-methylimidazole in chloroform using methyliodide, with $K_2CO_3 \cdot 1.5H_2O$ as a solid base. The purity of the cation was checked by elemental analysis and ^1H NMR in D_2O. The iodide salt was then transformed to the hydroxide by anion exchange in water solution using Dowex Monosphere 550 A (OH) anion resin (Aldrich). The hydroxide solution was concentrated by rotovaporation under vacuum and with mild heating. The final concentration was determined by titration using a certified HCl solution and phenolphthalein. For the zeolite synthesis, tetraethylorthosilicate was hydrolyzed under stirring in the hydroxide solution. All the ethanol and some water were allowed to evaporate. Then, the remaining amount of water was monitored by weight and adjusted by adding more water. Finally, HF (39.3% recently titrated solution) was added and the thick gel formed was stirred with a spatula. The final composition was SiO_2/0.56 TMIOH/0.61 HF/14.2 H_2O. Crystallization was carried out at 175 °C for 28 days in Teflon vessels fitted into stainless steel autoclaves.

2.2. Characterization. The nature and phase purity of the crystallized solid before and after calcination at 750 °C for 6 h was monitored by

(15) Dovesi, R.; Saunders, V. R.; Roetti, C.; Orlando, R.; Zicovich-Wilson, C. M.; Pascale, F.; Civalleri, B.; Doll, K.; Harrison, N. M.; Bush, I. J.; Arco, P. D.; Llunell, M. *CRYSTAL06 User's Manual*; Università di Torino: 2006.
(16) Dovesi, R.; Orlando, R.; Civalleri, B.; Roetti, C.; Saunders, V. R.; Zicovich-Wilson, C. M. *Z. Kristallogr.* **2005**, *220*, 571−573.
(17) Pascale, F.; Zicovich-Wilson, C. M.; López-Gejo, F.; Civalleri, B.; Orlando, R.; Dovesi, R. *J. Comput. Chem.* **2004**, *25*, 888−897.
(18) Valenzano, L.; Torres, F. J.; Doll, K.; Pascale, F.; Zicovich-Wilson, C. M.; Dovesi, R. *Z. Phys. Chem.* **2006**, *220*, 893−912.
(19) Orlando, R.; Torres, J.; Pascale, F.; Ugliengo, P.; Zicovich-Wilson, C. M.; Dovesi, R. *J. Phys. Chem.* **2006**, *110*, 692−701.
(20) Pascale, F.; Zicovich-Wilson, C. M.; Orlando, R.; Roetti, C.; Ugliengo, P.; Dovesi, R. *J. Phys. Chem. B* **2005**, *109*, 6146−6152.
(21) Pascale, F.; Tosoni, S.; Zicovich-Wilson, C. M.; Ugliengo, P.; Orlando, R.; Dovesi, R. *Chem. Phys. Lett.* **2004**, *396*, 308−315.
(22) Zicovich-Wilson, C. M.; Pascale, F.; Roetti, C.; Saunders, V. R.; Orlando, R.; Dovesi, R. *J. Comput. Chem.* **2004**, *25*, 1873−1881.
(23) Prencipe, M.; Pascale, F.; Zicovich-Wilson, C. M.; Saunders, V.; Orlando, R.; Dovesi, R. *Phys. Chem. Min.* **2004**, *31*, 559−564.
(24) Maurin, G.; Bell, R. G.; Devautour, S.; Henn, F.; Giuntini, J. C. *Phys. Chem. Chem. Phys.* **2004**, *6*, 182−187.
(25) Sastre, G.; Fornes, V.; Corma, A. *J. Phys. Chem. B* **2002**, *106*, 701−708.
(26) Smirnov, K. S.; Bougeard, D. *Catal. Today* **2001**, *70*, 243−253.
(27) Lee, S. H.; Choi, S. G. *Bull. Korean Chem. Soc.* **1999**, *20*, 587−591.
(28) Gómez-Hortigüela, L.; Corà, F.; Catlow, C. R. A.; Pérez-Pariente, J. *J. Am. Chem. Soc.* **2004**, *126*, 12097−12102.
(29) Smirnov, K. S.; Bougeard, D.; Tandon, P. *J. Phys. Chem. A* **2006**, *110*, 4516−4523.
(30) Lo, C.; Trout, B. L. *J. Catal.* **2004**, *227*, 77−89.
(31) Lazzeri, M.; Mauri, F. *Phys. Rev. Lett.* **2003**, *9003*, 6401−6401.
(32) Ricchiardi, G.; Damin, A.; Bordiga, S.; Lamberti, C.; Spano, G.; Rivetti, F.; Zecchina, A. *J. Am. Chem. Soc.* **2001**, *123*, 11409−11419.
(33) Arean, C. O.; Nachtigallova, D.; Nachtigall, P.; Garrone, E.; Delgado, M. R. *Phys. Chem. Chem. Phys.* **2007**, *9*, 1421−1436.
(34) Bulanek, R.; Drobna, H.; Nachtigall, P.; Rubes, M.; Bludsky, O. *Phys. Chem. Chem. Phys.* **2006**, *8*, 5535−5542.
(35) Nachtigall, P.; Bulanek, R. *Appl. Catal., A* **2006**, *307*, 118−127.
(36) Pidko, E. A.; Xu, J.; Mojet, B. L.; Lefferts, L.; Subbotina, I. R.; Kazansky, V. B.; van Santen, R. A. *J. Phys. Chem. B* **2006**, *110*, 22618−22627.
(37) Nachtigallova, D.; Bludsky, O.; Arean, C. O.; Bulanek, R.; Nachtigall, P. *Phys. Chem. Chem. Phys.* **2006**, *8*, 4849−4852.
(38) Sierraalta, A.; Hernandez-Andara, R.; Ehrmann, E. *J. Phys. Chem. B* **2006**, *110*, 17912−17917.
(39) Nachtigall, P.; Garrone, E.; Palomino, G. T.; Delgado, M. R.; Nachtigallova, D.; Arean, C. O. *Phys. Chem. Chem. Phys.* **2006**, *8*, 2286−2292.
(40) Bucko, T.; Hafner, J.; Benco, L. *J. Chem. Phys.* **2004**, *120*, 10263−10277.

powder X-ray diffraction (Bruker D-8 powder diffractometer) using Cu Kα radiation. Infrared spectra in the 4000−200 cm^{-1} range were recorded in a Nicolet FT-IR 20SXC spectrophotometer using the KBr pellet technique. The Raman spectra were recorded in a Renishaw Ramascope 2000 microspectrometer with an excitation wavelength of 514.5 nm.

3. Computational Details

3.1. Methodology. All calculations have been performed using the periodic approximation as implemented in the CRYSTAL06 code.[15] Accordingly, both, as made and calcined ITQ-12, have been considered as perfect crystalline structures with a primitive cell of 12T framework sites. The reported crystallographic cell is in both cases monoclinic (space group: *C*1*m*1),[14] but in the as-made material the symmetry mirror plane appears owing to the existence of two most probable orientations of the asymmetric TMI^+ molecule that are specular images to each other and equiprobable, giving rise to a global *pseudo*-symmetry. As a matter of fact, a more complex situation might actually occur, since a thorough inspection indicates that the TMI^+ molecule could adopt four nearly equivalent orientations, related to each other by means of the previously mentioned mirror plane, a perpendicular C_2 axis, and the resulting inversion center. According to this, the pseudo-symmetry of the cage contents in the as-made crystal would match the topological symmetry of the ITW framework, namely*C*12/*m*1.

In our model of the as-made material we have made the following choices:

1. Assuming that the random distribution along the four possible orientations of the SDA indicates that the framework distortions around the obloid cavity are similar in all cases and localized enough into a single unit cell so as to just slightly perturb the neighboring cells, all molecules are equally oriented in the model considered, keeping the maximum periodicity at the expense of losing the pseudo-symmetry elements.

2. After the previous choice the crystal becomes triclinic. However, in order to represent the pseudo-symmetry constraints imposed by the disordered template orientation, the cell parameters have been kept fixed into the experimental monoclinic values.

Concerning the calcined material, the cell parameters have been also kept fixed into the experimental monoclinic values for the sake of consistency with the choices considered for the as-made material. The remaining degrees of freedom (the atomic positions) have been fully optimized (under *C*1*m*1 symmetry constraints in the calcined material), considering the experimental structures as the starting point of the optimization process. Nevertheless, in order to check the extent of validity of the previous approximations, fully optimized structures have been also considered for the sake of comparison with the constrained ones. Both types of calculations are in the following referred to as fixed cell and optimized cell calculations, respectively.

All calculations have been performed at the B3LYP density functional level of theory.[41,42] The exchange-correlation functional was numerically integrated over an unpruned grid of points. The integration was performed using 55 radial and 234 angular points, generated through the Gauss−Legendre and Lebedev schemes, respectively. A Pack−Monkhorst shrinking factor of 2 and the default integral evaluation parameters documented in the code manual[15] have been adopted. A basis set of quality DZV with polarization on some selected atoms has been considered. For C, N, H a standard 6-31G basis set has been used. F and O atoms have been represented with modified 6-31G* basis sets, in which the corresponding sets of modified exponents are $\{\alpha_d = 0.3\ \text{bohr}^{-2}\}$ and $\{\alpha_{sp} = 0.279\,84\ \text{bohr}^{-2}, \alpha_d = 0.5\ \text{bohr}^{-2}\}$, respectively. In the case of Si, a modified 6-21G*, $\{\alpha_{sp} = 0.13\ \text{bohr}^{-2}; \alpha_d = 0.5\ \text{bohr}^{-2}\}$ has been used. Geometry optimizations have been performed using analytical gradient techniques for both atomic positions and lattice parameters.[15,43]

Vibrational modes and their corresponding frequencies have been computed by means of numerical second derivatives of the total energies as implemented in the CRYSTAL06 code.[15,17] The IR intensities are calculated according to

$$I_i^{\mathrm{IR}} \propto \sum_{\alpha} \left(\sum_{A\beta} Z^*_{A,\alpha\beta}\, e_{i,A\beta} \right)^2 \tag{1}$$

where $e_{i,A\beta}$ is the contribution of coordinate β on atom A to the i-th normal mode and $Z^*_{A,\alpha\beta}$ is the Born dynamic charge tensor, defined as

$$Z^*_{A,\alpha\beta} = \frac{\partial \mu_\alpha}{\partial x^A_\beta} \tag{2}$$

where μ_α and x^A_β are the components of the dipole moment and the coordinates of atom A, respectively.

Indeed, in crystalline systems the dipole moment is not a bulk property as its value would depend on the arbitrary choice of the unit cell. On the contrary, the dipole moment difference between two geometries of the same system, the polarization per unit cell, can be computed without arbitrariness, being a well-defined observable in periodic systems. Exploiting this fact, the partial derivatives involved in eq 2 are estimated numerically from the polarizations generated by small atomic displacements, the same ones as considered for the calculation of the energy second derivatives. This strategy is performed by adopting the localized Wannier Function (WF) approach to compute polarizations, a technique implemented in previous versions of the code and already discussed in detail.[44−46] In this approach, the polarization is computed as a difference between the sum of the centroids of the reference localized WFs obtained at each geometry.

In the present implementation, the procedure for the calculation of the centroids and the WFs has slight modifications with respect to that used in the above-mentioned works. At the central point, the WFs and its centroids are computed by means of the usual intrinsic localization scheme.[46] Nevertheless, at the displaced geometry points, they are obtained through projections of the WFs calculated at the central point onto the corresponding occupied manifolds. Owing to the small geometry differences between the central and the displaced points in the atomic coordinate space, the projection technique permits us to obtain localized enough WFs suitable for the accurate computation of the polarization, providing a significant gain in computational cost with respect to the adoption of the intrinsic localization scheme at each point.

3.2. Classification of the Vibrational Modes. The classification of the vibrational modes in crystals with large unit cells is a quite cumbersome task owing to the large number of degrees of freedom and the quite delocalized character of the motions involved. In previous works of some of us, devoted to the study of the vibrational modes of minerals of the Garnet family,[19,20] the mode characterization has been performed in terms of the motions of quite delimited and independent substructures. This scheme is not fully applicable to the case of zeolites where frameworks consist of semi-covalently bonded atoms and should be in principle considered as a whole. It appears that the motions of the different structural pieces in a given vibrational mode are closely related to each other featuring a quite global behavior.

Nevertheless, a generalization of this scheme through a description in terms of framework Building Units (BUs) seems to be the best way to rationalize the normal modes even in this quite difficult case where

(41) Becke, A. D. *J. Chem. Phys.* **1993**, *98*, 5648−5652.
(42) Lee, C.; Yang, W.; Parr, R. G. *Phys. Rev. B* **1988**, *37*, 785.
(43) Doll, K.; Saunders, V. R.; Harrison, N. M. *Int. J. Quantum Chem.* **2001**, *82*, 1−13.
(44) Baranek, P.; Zicovich-Wilson, C. M.; C. Roetti, R. O.; Dovesi, R. *Phys. Rev. B* **2001**, *64*, 125102.
(45) Noel, Y.; Zicovich-Wilson, C. M.; Civalleri, B.; D'Arco, Ph.; Dovesi, R. *Phys. Rev. B* **2001**, *65*, 014111.
(46) Zicovich-Wilson, C. M.; Dovesi, R.; Saunders, V. R. *J. Chem. Phys.* **2001**, *115*, 9708−9719.

Table 1. Energies Per Primitive and Conventional Cell Parameters of the Fixed Cell and Fully Optimized Structures[a]

	calcined		as-made	
	cell opt	cell fix	cell opt	cell fix
a	10.3444	10.3360	10.5631	10.4478
b	15.1968	15.0177	15.1516	14.9854
c	8.9844	8.8639	8.9238	8.8366
α	89.56	90.00	89.38	90.00
β	105.39	105.36	105.97	105.94
γ	89.77	90.00	89.78	90.00
volume	1361.65	1326.76	1372.97	1330.34
energy[b]	−0.42382	−0.42011	−0.72601	−0.71925

[a] Energies in hartree, length in Å, angles in degrees. [b] Reference energies per primitive cell for calcined and as-made are −5280 and −5724 hartrees, respectively.

the BUs always share at least one atom. In the present work, framework vibrations are characterized in terms of those BUs customarily adopted in the topological description of zeolites.[5] Two different families are considered to this scope namely, the set of primary BUs (SiO_4 units) per unit cell, and a set of rings that fully cover the two main cavities: D4R and 8R-CI (see Figure 1). The labels that identify the 14 building rings per unit cell are shown in Figure 3.

The classification and description of the vibrations according to the previous considerations is here performed through a quantitative partition of the modes into external and internal BU contributions, as it is shown in the Appendix.

Concerning the organic guest and the fluoride anion, their modes are described according to the usual conventions for molecules.

4. Results and Discussion

4.1. Optimized Structures. In order to explore the limits of the fixed cell approach considered in this work, let us first compare the energies and cell parameters of the calcined and as-made ITQ-12 obtained upon full and constrained optimizations. These data are documented in Table 1.

The cell distortion experimented by the fully optimized calcined structure is apparent in the increase of all cell lengths compared to the fixed (experimental) cell; particularly in *b* and *c*, whose changes are of about 1.2−1.4%, which gives rise to an increase of 2.8% in volume. It is worth noting that the full minimum loses the monoclinic symmetry as α and *β* slightly differ from the ideal 90° angles. These changes arise without a significant energy decrease (0.2 kcal·mol^{-1} per SiO_2). Therefore, the results strongly suggest that the monoclinic phase of ITQ-12 is not the most stable one, and it is resolved from powder diffraction experiments as a kind of average provoked by lattice vibration at room temperature. This matter is also supported by the vibration analysis given in the Supporting Information.

As regards the as-made sample, all three cell lengths are overestimated in the optimized structures giving rise to an increase of 3% in volume. This systematic trend in overestimating the cell volumes of both, the calcined and the as-made materials, may be a consequence of the methods considered here for calculations, as it is well-known that B3LYP tends to slightly overestimate Si−O distances.

In what concerns the triclinic distortion of the as-made structure and at variance with the case of the calcined ITQ-12, an additional factor of disorder is present in the experiments owing to the random distribution of the four orientations of the TMI^+ cation in the cavity, discussed above. Conversely one can say that, despite the artificial order imposed in our model, the resulting triclinic distortion is actually quite small, suggesting

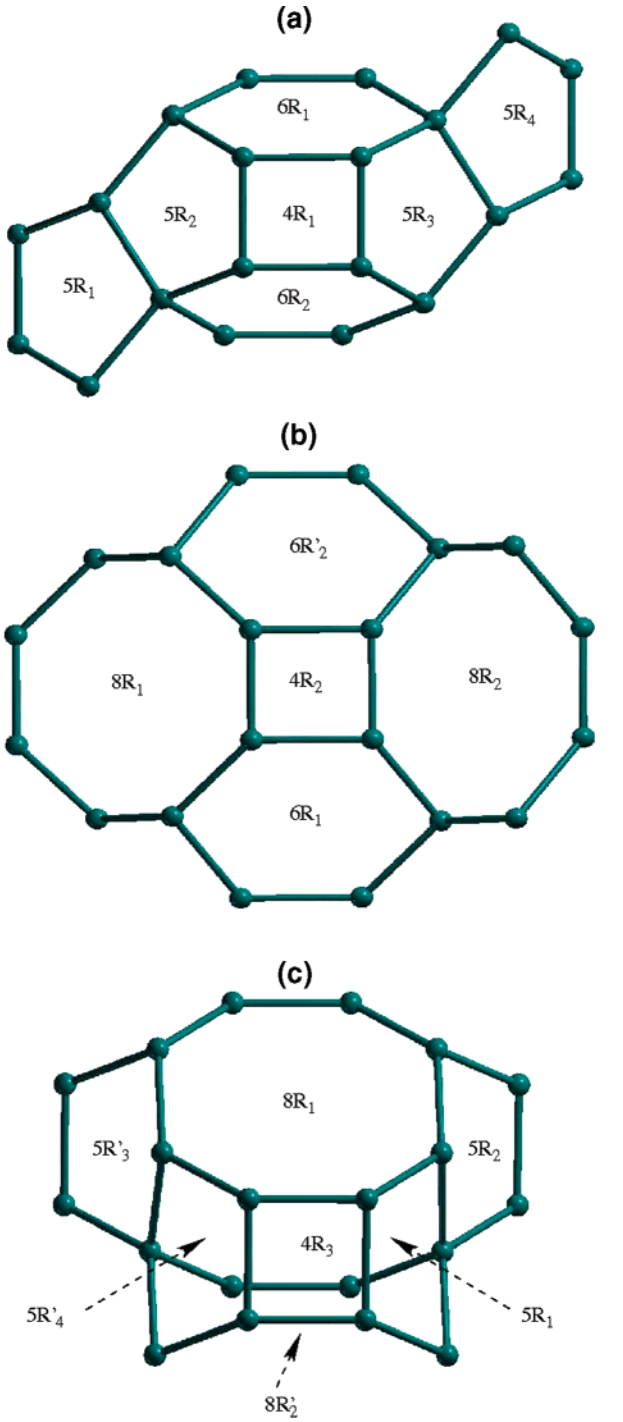

Figure 3. Convention adopted to label ring units in ITQ-12. Views of the 8R-CI cavity are given with reference to Figure 1: (a) front, (b) top, and (c) left. Primed labels indicate the rings are located in a different primitive cell than those appearing in panel (a). Rings $4R_{4-6}$, not visible in the figures, are at the opposite side of $4R_{1-3}$ in the D4R unit, respectively.

that the SDA orientation is not determinant for the stability of the synthesized crystal, which supports the assumptions taken for our model choice. In the same direction go the results on total energies for the cell optimized and cell fixed calculations. A very small stabilization is experimented by the fully optimized (triclinic) model, with an energy difference of the same order as that featured by the calcined material.

Despite the above-discussed discrepancies between the experimental and optimized cell parameters, it is remarkable that

Table 2. Standard and Maximum (in Parenthesis) Deviations of Internal Coordinates between Experimental and Optimized Structures (Distances in Å, Angles in deg)

	calcined	as-made
Si−O	0.018 (−0.028)	0.021 (−0.033)
O−Si−O	5.94 (13.39)	5.76 (13.62)
Si−O−Si	10.56 (−18.68)	6.57 (18.15)
Si−O−Si−O	43.42 (101.95)	30.10 (−71.74)
Si−O−Si−O[a]	33.01 (−66.76)	17.73 (47.26)
Si−O−Si−O[b]	58.96 (101.95)	45.69 (−71.74)
X−X[c]		0.028 (−0.062)
X−X−X[c]		1.51 (2.44)
X−X−X−X[c]		1.27 (−2.05)

[a] The central Si belong to the D4R. [b] The central Si does not belong to the D4R. [c] X represents either C or N.

both sets of data display the same qualitative behavior in going from the as-made to the calcined materials. It arises from data listed in Table 1 that an apparent decrease of parameter *a* is accompanied by a slight increase of *b* and *c* upon calcination. The total volume decreases in about 1%. This effect has been previously explained as due to the filling of the obloid cavity brought about by the presence of the TMI^+ molecule.[14]

A general conclusion is that the fixed cell constraint imposed on both models does not carry a significant error in the representation of the actual calcined and as-made ITQ-12, and, in addition, it allows to take into account in the models some averaged constraints imposed by disorder in the global systems.

Considering just those structures optimized with a fixed cell, let us now pay attention to the differences between the optimized internal coordinates and the experimental ones. In Table 2 the standard and the maximum deviation between these sets of data are reckoned. Obviously, those coordinates involving H atom positions are not considered, as experimental data are not available.

In what concerns the inorganic part, it arises that the larger differences are displayed by the O-bridge angles (Si−O−Si) and the corresponding dihedral angles (Si−O−Si−O) that feature mean distortions of more than 10° and 40°, respectively. The maximum differences are very large in the case of the dihedral angles with a value of 102°. Although this difference is quite large, it does not actually involve a significant change of the relative atomic positions, but just a rotation of a Si−O−Si bridge with quite a large angle. This situation is shown in Figure 4.

As concerns the organic part, differences are within the range expected according to the dissimilar approximations considered in simulations and refinements of experimental XRD pattern, as it is discussed in what follows. However, a remarkable fact is that the molecule orientation and position inside the obloid cavity obtained by geometry optimization is very similar to one of the two geometries obtained from diffraction data, validating both the assumptions made in the structure refinement[14] and the suitability of the adopted theoretical method.

On the other hand, it is worth noting that the optimized geometries support the experimental result in what concerns the slight deformation from flatness of the occluded molecule, which is an indication of a slight loss in aromaticity of the imidazol ring. As a matter of fact, the standard deviations of the dihedral angles with respect to the planar values are of 0.33° and ∼0° for the occluded and free TMI^+, respectively, using the same methodology and program. This loss of flatness of the molecule

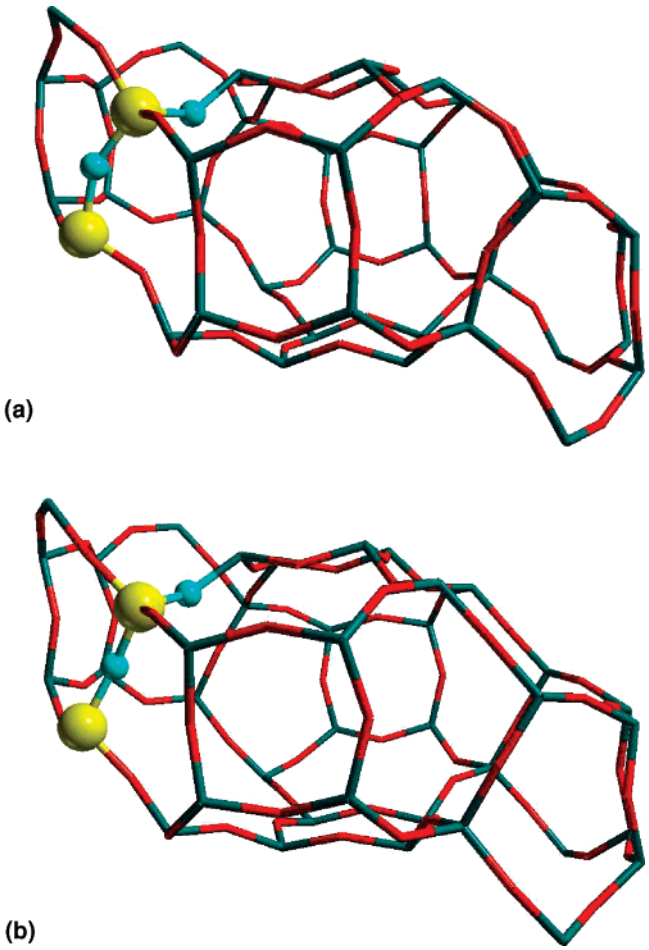

Figure 4. Representation of the 8R-CI for the calcined material at the experimental (a) and the optimized (b) geometries. The highlighted atoms belong to the dihedral angle that changes 102° in the optimization (see Table 2).

can be interpreted as given rise by a non-negligible spatial confinement inside the rather narrow obloid cavity.

The most distorted framework parameters, the angles and dihedrals between SiO_4 units sharing one O atom, are actually the most flexible ones in zeolitic frameworks, as their variation does not carry a significant energy change.[47,48] Therefore, the quite large allowed distortion along such geometrical parameters with practically no energetic cost indicates a significant framework flexibility of ITQ-12 expedited by the fact that its particular topology seems not to impose strong constraints onto the soft or "floppy" modes.[47] It is worth noting that this flexibility is larger for the tetrahedral units that do not participate in the D4R unit than for the others (see Table 2), as expected owing to the highly constrained geometry of the units. From the results given in Table 2, it can be indirectly deduced that the presence of the template decreases the overall framework flexibility, as the differences of these floppy geometrical parameters between the experimental and optimized structures are not as significant as in the calcined material.

Owing to this large structural flexibility, it is not expected that the atomic positions obtained through the Rietveldt refinement of diffraction data and the B3LYP optimization do

(47) Hammonds, K. D.; Heine, V.; Dove, M. T. *J. Phys. Chem. B* **1998**, *102*, 1759−1767.
(48) Sartbaeva, A.; Wells, S. A.; Treacy, M. M. J.; Thorpe, M. F. *Nat. Mater.* **2006**, *5*, 962−965.

Table 3. Closest (<2.6 Å) OH Distances between the Framework and the Template[a]

methyl	rings	distance
1	$6R_1/8R_1$	2.507
1	$6R_2/8R_2$	2.591
1	$4R_5/6R_2$	2.597
3	$4R_5/6R_1$	2.466
3	$6R_1/8R_1$	2.522
3	$6R_2/8R_2$	2.553
4	$6R_2/8R_2$	2.441
4	$5R_1/8R_1$	2.462

[a] The position of the methyl group in the imidazolium ring (1 and 3 are N), the framework rings to which the O belong (see Figure 3), and the distances in Å are the vertical entries.

coincide. This is because, while the latter gives the geometry at 0 K (minimum energy structure), the former is the result of an averaging performed not on atomic positions but on interplanar distances that should actually provide different results with a dependence on temperature.

Finally, let us consider the positions of the H atoms in the most stable geometry of TMI-F-ITQ-12 according to the present B3LYP calculations, information which is not available from XRD experiments. As previously reported,[14] the methyl groups of the TMI^+ are mostly directed toward the equatorial walls of the obloid cavity. From the B3LYP optimized geometries and using our previously defined notation (see Figure 3), the methyl groups in positions 1 and 3 are apparently directed toward $5R_3$ and $4R_4$, respectively, while that in position 4 roughly points to the intersection among $8R_1$, $5R_2$, and $4R_6$. Owing to this orientation of the template, the two less acidic methyl groups (bonded to N in the ring) are located in an environment rich in O atoms, while the group in position 4, though displaying the largest number of OH contacts <2.5 Å, resides in a region with a low number of framework O atoms, as it is close to the eight-ring opening of the 8R-CI unit. The contact distances between the methyl H and the framework O atoms are listed in Table 3. The environments of methyl groups 1 and 3 are quite similar, as they arise from the distances given in the table. Nevertheless there is a remarkable difference in that the shortest OH distance occurs in the latter in contact with an O belonging to one of the four-ring cages of the D4R unit, i.e., at the neighbors of the F^- anion. We shall go back to this issue later on in the discussion on the soft vibrational modes.

The atomic positions and cell parameters of all optimized structures are given in the Supporting Information.

4.2. Vibrational Analysis. The experimental and calculated IR frequencies and intensities of both the as-made and calcined monoclinic structures are shown in Figure 5 (numerical values of calculated results are given in the Supporting Information). A very good agreement between experimental and simulated absorption peaks is exhibited, with maximum differences of about 20 cm^{-1} in some exceptional cases. From the theoretical point of view, this supports the already well documented suitability of the B3LYP approximation to compute the vibrational frequencies of solids.[20,22,49,50] More relevant for practical purposes, this remarkable accuracy permits us to establish an unambiguous correspondence between theoretical modes and

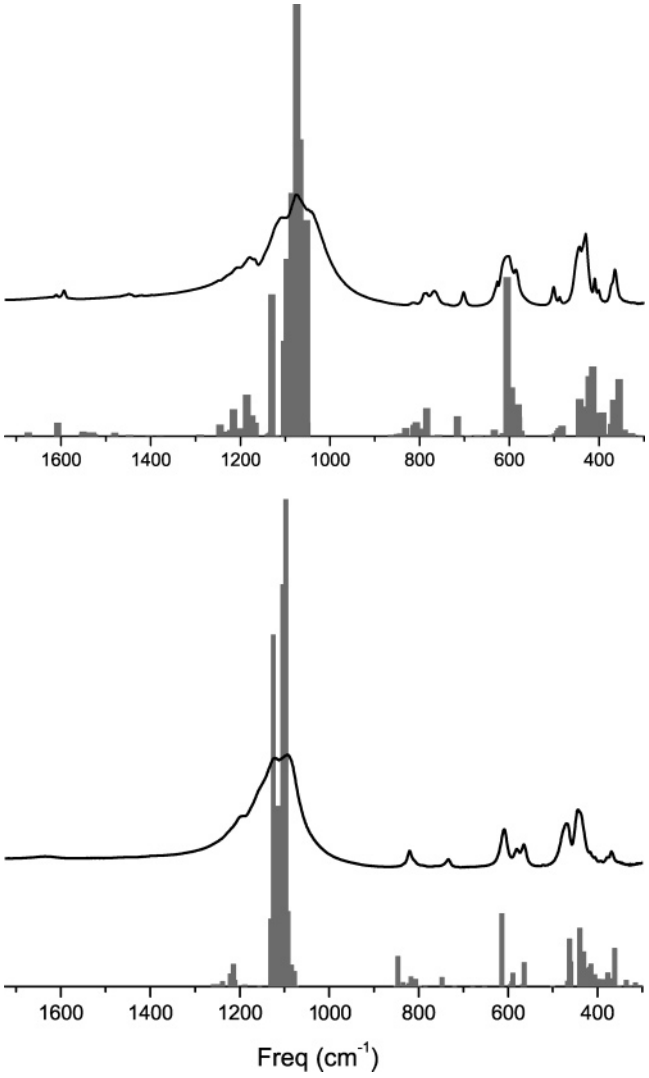

Figure 5. Experimental and simulated spectra for as-made (top) and calcined materials (bottom). Gray bars refer to B3LYP frequencies and intensities. Experimental spectra recorded at 298 K.

experimental peaks making possible the full assignation of the spectra. This is often a very hard task for large and complex structures like zeolites owing to the high density of modes displayed by the spectra in several zones, which makes difficult an assignation based on frequency values obtained from not accurate enough theoretical methods.

In spite of the structural resemblances, it is difficult to establish a clear correspondence between the framework modes of the calcined and the as-made materials. This is a result of the remarkable perturbation of the framework vibration in the presence of the SDA and F^- that gives rise to a large mixing of the normal modes of the clean inorganic lattice.

As the analysis of all modes is a very hard task and, maybe, not very fruitful, let us focus on those modes that can give some insight on the phenomena related to the structure-directing effect of the extraframework species. To this scope it is worthwhile to initially pay attention to the richest and most complex part of the vibrational spectrum that is the zone of lowest frequencies (<500 cm^{-1}). In order to facilitate this analysis one will make use of the decomposition of the modes into external/internal contributions of the BU motions discussed in section 3.2 and developed in the Appendix.

(49) Montanari, B.; Civalleri, B.; Zicovich-Wilson, C. M.; Dovesi, R. *Int. J. Quantum Chem.* **2006**, *106*, 1703−1714.
(50) Labéguerie, P.; Pascale, F.; Mérawa, M.; Zicovich-Wilson, C.; Makhouki, N.; Dovesi, R. *Eur. Phys. J. B* **2005**, *43*, 453−461.

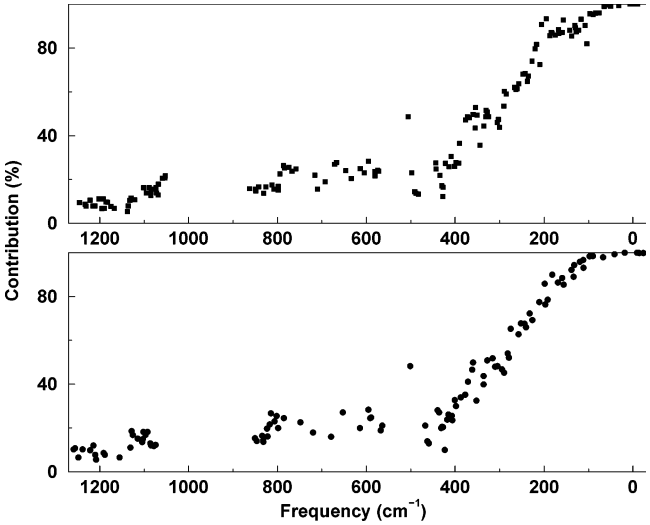

Figure 6. Total external contributions to the vibrational modes according to a partition in terms of SiO_4 units. Bottom and top panels correspond to the calcined and as-made materials, respectively.

As concerns the decomposition in terms of SiO_4 units, the results are shown in Figure 6, where the total external contributions from the primary tetrahedral units to the *i*-th mode, Ξ_i [see eq 5], in the calcined and as-made materials against their frequencies are given. The analysis of the external contributions of the SiO_4 units gives an idea of the extent to which they behave rigidly along the motion. These results are complemented by the contributions from the extraframework species given in Figure 7. Only modes of frequency less than 1280 cm^{-1} are considered; beyond this value all modes display 100% of extraframework character.

The external contribution from the framework tetrahedral units decreases as increasing the frequencies in a rather monotonous way, bearing resemblance to a sigmoid function. At very low frequencies this contribution is practically constant (100%), while in the range 200−500 cm^{-1} it decreases *quasi*-linearly. This frequency region is usually attributed to Si−O−Si bending and O−Si−O−Si torsions between different SiO_4 units. At larger frequencies, comprising the O−Si−O bending and Si−O stretching regions, 550−900 cm^{-1} and 1000−1280 cm^{-1}, respectively, there is a slow decrease of contributions external to the tetrahedral units.

As expected from previous studies[47,48,51,52] there are several normal modes that practically behave as rigid unit modes with close to 100% of the external motion of the tetrahedral units whose number should depend on the framework topology and, thereby, flexibility. The set obviously includes not only the pure translations but also the phase transition in the calcined ITQ-12 (represented in the figure with negative frequency; see discussion in the Supporting Information) indicating that this process mainly involves a change in the "packing" of the SiO_4 tetrahedra with practically null distortion of the units.

The vibrational modes feature almost rigid tetrahedra motions at frequencies lower than 100 and 60 cm^{-1} for the calcined and the as-made structures, respectively. Moreover, as it turns out from Figure 7, most modes of the as-made material in the region 60−300 cm^{-1} have a remarkable contribution from the extraframework species, which makes a significant difference with respect to those in the calcined zeolite.

Of particular interest is that the fluoride contributions are maximal within the range 100−160 cm^{-1}, which is also a region where large differences between the SiO_4 external contributions of the two systems appear. The SiO_4 units of the as-made material display a less rigid behavior in this zone with respect to the calcined one, exhibiting an apparent depression of more than 10% in the graphic shown in Figure 6.

As the relative rigidity of the framework tetrahedral units is mainly due to the directionality of the SiO bond conferred by its partially covalent character, the increase in flexibility observed at 100−160 cm^{-1} in the as-made material is expected to be accompanied by an increase in ionicity of the SiO bond. This suggests that the extraframework species in the as-made material feature an interaction with the zeolite inner surfaces that is much more complex than the short-range repulsion usually invoked to explain the structure directing action in terms of cavity filling. As a matter of fact, some extent of charge transfer does occur between these species and the framework in order to explain the vibrational behavior. This issue will be discussed further on from the point of view of the Born Dynamic Charges.

Another manifestation of the influence of the extraframework species on the framework vibrational modes appears in the 450−500 cm^{-1} frequency range. As it turns out from Figure 7, the three vibrational modes in this region display significant contributions from both F^- and TMI^+ in the as-made structure that are accompanied by a hypsochromic shift with respect to the clean material. The modes at frequency values 459, 463, and 468 cm^{-1} shift to 491, 483, and 498 cm^{-1}, respectively, in going from the calcined to the as-made ITQ-12. The main contribution to each mode is the antiphase breathing of a pair of opposite rings in the D4R unit, i.e., $4R_{1,4}$, $4R_{3,6}$, and $4R_{2,5}$, respectively, according to the labeling shown in Figure 3. All of them are active in IR, and the band has been already used for the characterization of the presence of F^- inside D4R units.[53] The band appears at about 500 cm^{-1} in all cases documented, and in the as-made ITQ-12 it is at 502 cm^{-1}, as it arises from Figure 5. In the calcined sample they appear as a more intense band around 460 cm^{-1}. The hypsochromic shift is attributable in this case to a decrease in the reduced mass of the mode owing to the additional contribution from the F^- and to the repulsion between the F^- and the O-bridging atoms of the 4MRs involved in the motion. As concerns the latter effect it has been shown in previous works[53,54] that this repulsion is not negligible owing to the remarkable confinement of the fluoride anion inside the D4R unit.

Regarding these motions it is also interesting to analyze the mode at 501 cm^{-1} in the calcined material (506 cm^{-1} in the as-made one). As it appears in Figure 6, the contribution from the external SiO_4 motion to this mode does not follow the trend of the whole set of data but displays an isolated increase of the rigid character of the tetrahedra. This mode features a breathing motion **in phase** of the 4MRs in the D4R unit with null contribution from the F^-. Owing to the latter fact, the small

(51) Hammonds, K. D.; Deng, H.; Heine, V.; Dove, M. T. *Phys. Rev. Lett.* **1997**, *78*, 3701.
(52) Hammonds, K. D.; Dove, M. T.; Giddy, A. P.; Heine, V.; Winkler, B. *Am. Mineral.* **1996**, *81*, 1057.
(53) Villaescusa, L.; Márquez, F.; Zicovich-Wilson, C. M.; Camblor, M. A. *J. Phys. Chem. B* **2002**, *106*, 2796−2800.
(54) George, A. R.; Catlow, C. R. A. *Chem. Phys. Lett.* **1995**, *247*, 408−417.

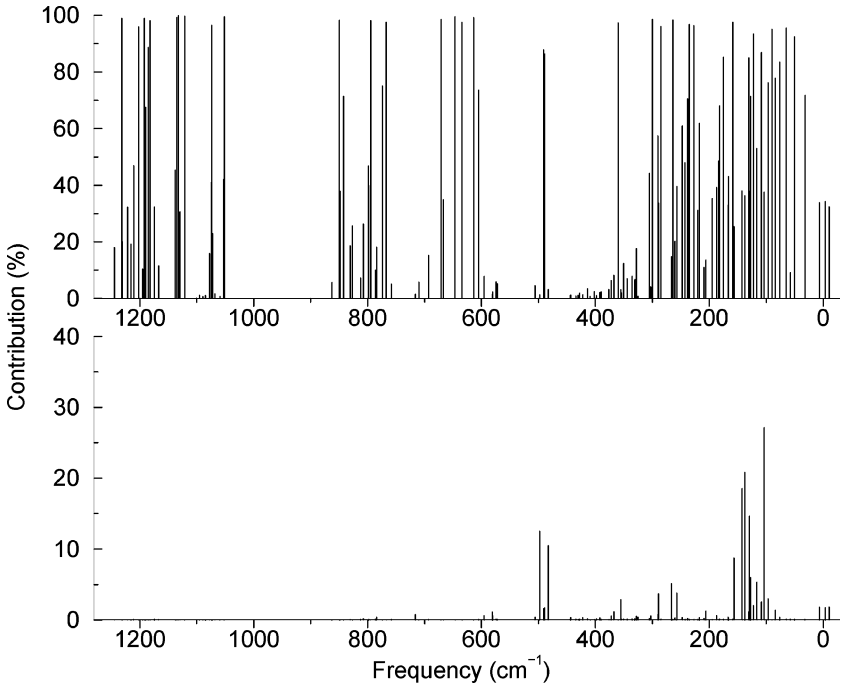

Figure 7. Figure 7. Contribution of the extraframework species to the as-made modes. Top, TMI^+; bottom, F^-.

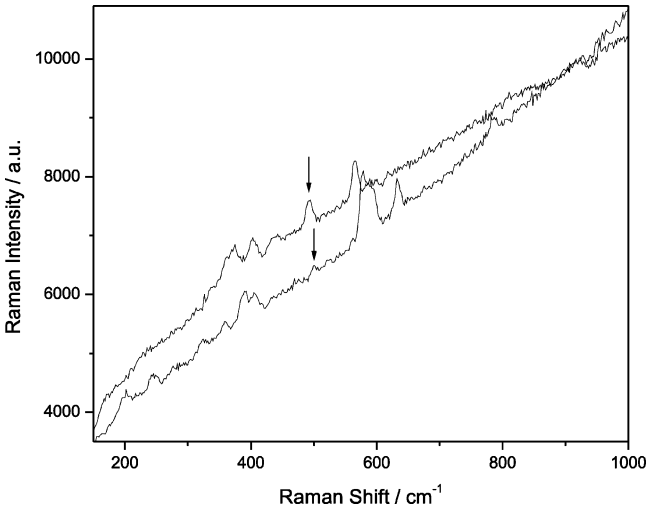

Figure 8. Raman spectra of pure silica zeolite ITQ-12: as-made (bottom) and calcined (top).

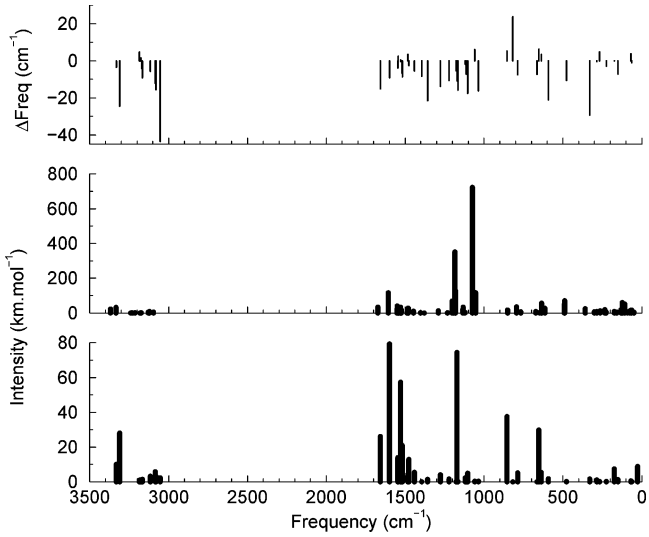

Figure 9. IR spectra of TMI^+. Bottom: Calculated in the gas phase. Middle: Calculated in the as-made ITQ-12 (bars). Top: Difference between the vibrational frequencies calculated for the gas phase and the as-made ITQ-12.

hypsochromic shift can only be ascribed to the F−O repulsion, providing evidence that this effect contributes to the shift of the other 4MR breathing modes in a lower amount than the decrease in the reduced mass. In this case, the quite uniform expansion and contraction of the D4R unit gives rise to less significant deformations of the tetrahedral units along the motion than in the related antiphase breathing modes which explains the more rigid behavior of the SiO_4 units. This vibration is practically inactive in IR, but it is clearly visible in the Raman spectrum of calcined ITQ-12 (494 cm^{-1}, Figure 8). The band is hardly detectable in the as-made sample, which may be due to the low quality of the spectrum caused by the strong fluorescence of the samples. This Raman band has been observed also in Octadecasil, another material whose structure contains D4R rings.[53]

Let us now compare the vibrational spectra of the TMI^+ molecule in the gas phase and occluded into the zeolite. Despite the fact that extraframework species contribute in most of the vibrational modes of the as-made material, it is worth noting that those that feature a contribution of more than 80% of the extraframework atoms are exactly 60, which corresponds to the number of degrees of freedom of the 20 atoms of the TMI^+ F^- complex. As it is shown in Figure 7 the difference between framework and extraframework modes is in general quite apparent in terms of these contributions. Taking these modes into consideration, in Figure 9 they are compared to those calculated for TMI^+ in the gas phase.

By looking at the difference between the calculated frequencies of the free and the occluded TMI^+, it turns out that most modes in the as-made material are blue-shifted with respect to the gas-phase ion, as the frequency differences between the latter and the former are predominantly negative. The average value

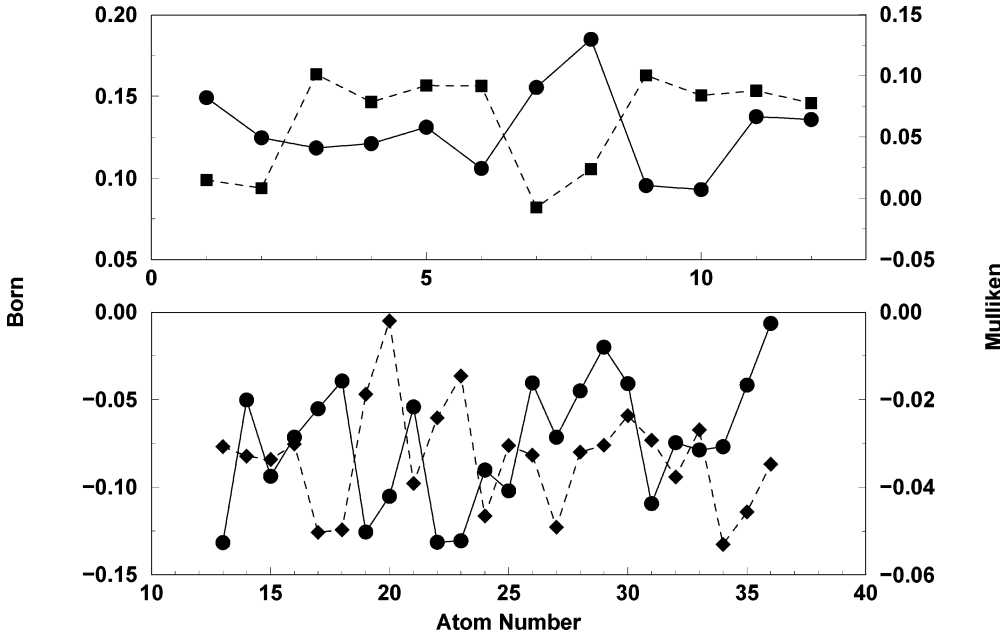

Figure 10. Differences in charges (in $|e|$) of framework atoms between as-made and calcined materials. Top and bottom panels: Si and O atoms, respectively. Circles and squares: Born and Mulliken charge differences, respectively. The atomic labels follow the ones used in the list of atomic positions given in the Supporting Information.

of the shift is about -20 cm^{-1}, while the maximum value of -43 cm^{-1} is featured by the 4-methyl C−H modes at ∼3100 cm^{-1}. These C−H frequencies are not corrected by anharmonicity; therefore they are not suitable to be compared with experimental values. Anyway, from the semiquantitative point of view, the larger shift of the C−H stretching modes on 4-methyl can be related to the larger acidity and the closer contact with the surface oxygen atoms, according to the considerations given in the previous paragraph.

4.3. IR Intensities and Dynamic Charges. According to Figure 5 it appears that the calculated and experimental IR intensities compare quite well, despite the former corresponds to the limiting case at 0 K, while experiments were actually performed at room temperature.

It turns out from both sets of data that the largest intensities in the spectra are featured by those modes whose frequencies are in the range between 1000 and 1170 cm^{-1} which chiefly correspond to Si−O stretching motions. The high intensity is due to the significant change in dipole moment featured by the SiO bonds as the distance between the atoms increases in going toward heterolytic dissociation.

A much more surprising fact is that in the as-made material the differences in intensity between the SiO stretching band and the remaining modes lower with respect to the calcined material. A first explanation can be drawn by attributing this equalization to the participation of the charged TMI^+ and F^- in most modes, which does increase their dipole moment change and, accordingly, the IR intensity. However, an analysis of the Born dynamic charges, defined as the averaged diagonal elements of the tensor given in eq 2, shows that a more complex phenomenon is possibly involved.

It is worth noticing that, as a difference with the Mulliken partition of the electron density, the Born dynamic charges correspond to a macroscopic observable which provides the effective charges that should be attributed to each atom so as to reproduce the dipole moment changes brought about by small structural distortions. By definition the sum of all dynamic charges per cell must be zero.

The Born charges computed for F^- and the TMI^+ fragment as a whole are -1.20 and $1.43|e|$, respectively. While these values depend on a variety of electronic processes that take place during the motion of the atoms (polarization, electron transfer, etc.), it is remarkable that in both cases the dynamic charges exceed in magnitude the formal charges of the free ions. The only way this could occur is when the most probable motions of the ions are accompanied by a certain degree of charge transfer (or electron density polarization) either toward or from the neighboring atoms. In the present case, this means that the occluded ionic fragments dynamically exchange electrons with the framework atoms.

As a matter of fact, the framework atoms display significant differences between the calcined and the as-made materials in their dynamic and static charges, as it arises from Figure 10. Both Born and Mulliken charges make apparent that the framework turns to be more ionic in the presence of the SDAs; i.e., O and Si atoms become more negative and positive, respectively in the as-made material, confirming the increased ionicity of the Si−O bond commented on above. Despite this general trend, a detailed analysis of the data represented in Figure 10 shows that both charge partitions display different trends in what concerns the atomic contributions, which is to be partially attributed to the influence of the dynamic nature of the interactions.

For instance, by looking at the Si atoms, those that display the largest differences in the static charges between the as-made and calcined materials are the ones labeled by numbers from 3 to 6 and 9 to 12 in Figure 10 (highest values in the top panel), apparently influenced by the presence of the F^- anion, as they are at the corners of the D4R unit. This phenomenon is to be associated to the above-discussed loss of SiO_4 external character (hence increased internal flexibility) of the modes in the 100−200 cm^{-1} range in the as-made ITQ-12. In fact, while the mean

quadratic deviation from perfect tetrahedrality is about 0.9° for those D4R-SiO_4 units in the calcined material, this value increases to 4.5° in the as-made sample, while the remaining tetrahedra practically do not change (see Table S7). These results strongly support the evidence that the presence of the occluded F^- allows an additional relaxation of the tetrahedra in the D4R units, due by an increase in ionicity, giving rise to a global effect that favors their formation in materials crystallized through the fluoride route, while the effect would be missing in the hydroxide route.

This important result is to be related to previous findings[55,56] in which it has been shown that the presence of framework cations more ionic than Si (for instance Ga and Ge) gives rise to stabilization of those framework units that exhibit a large density of 4-MR. This is because the increased ionicity allows the TO_4 tetrahedra to feature slight deformations that allow an efficient structural relaxation, not possible with the more rigid SiO_4 units in small rings.

As concerns the dynamic Born charges, a detailed analysis of their differences between calcined and as-made materials is given in the Supporting Information. It is worth noting that the O atoms that display the largest differences in the Born charges between as-made and calcined materials are probably polarized or featuring some amount of electron transfer with the SDA due to the vibrational motions that approach them to the TMI^+ hydrogen atoms bringing about temporary hydrogen-like interactions. This effect can be related to the fact that the mode at 1073 cm^{-1} exhibits a remarkably larger intensity in the zeolite cavity than in the gas phase. This mode features H−C−C and H−C−N bending together with a kind of imidazolium breathing mode, and the substantial change in the dipole moment during the motion, revealed by the IR intensities shown in Figure 9, would indicate a charge-transfer process with the framework is taking place.

5. Conclusions

A detailed structural and vibrational characterization of the as-made and calcined forms of zeolite ITQ-12 based on periodic B3LYP calculations has been provided. The monoclinic symmetry previously reported for the calcined material is slightly unstable, while disorder arising from different orientations of the organic SDA may justify the average monoclinic symmetry of the as-made material. The calculated structures agree with the experimental observation in that the zeolite contracts anisotropically on calcination, with a significant decrease in the *a* parameter, which could be related to the filling of the obloid cavity by the SDA. The optimized SDA structure also agrees substantially with that derived from powder diffraction analysis, but the calculations allow us to locate the hydrogen atoms and to identify close interactions with certain framework oxygen atoms.

The calculated infrared spectra show an outstanding agreement with the experimental ones, in terms of both frequencies and relative intensities, which is considered a consequence of the high level of theory employed as well as of the good quality of the defect-free pure silica samples. A soft mode with an imaginary frequency in the spectrum of the monoclinic model of the calcined material confirms the stability issue and is associated to the triclinic−monoclinic transition. The low value of its imaginary frequency suggests that at RT a fast exchange between two triclinic phases results in an averaged monoclinic symmetry at the time scale of the X-ray diffraction experiments.

A detailed vibrational analysis based on a partition of each vibrational mode into internal and external contributions of building units (both SiO_4 tetrahedra and discrete rings) reveals important features concerning framework flexibility and host−guest interactions in these materials. Several normal modes behave as rigid unit modes, with close to 100% contribution of motions external to the tetrahedral units, but the rigidity of the tetrahedral units in the as-made zeolite is lower than that in the calcined material. This is attributed to an increased ionicity of the Si−O bonds in the former, supported by the analysis of the soft vibrational modes, the IR intensities, and the Born and Mulliken charges, in which the occluded F^- appears to be mainly responsible.

The increase in ionicity brought about by the occluded extraframework species in the as-made zeolite may be a key point in explaining the peculiar structure-directing effect of the F-route toward pure silica zeolites with D4R, which have not been crystallized so far by the traditional OH-route.

The present results provide, for the first time in the zeolite literature, strong theoretical evidence that the role of occluded F^- in the synthesis of these materials is similar to that of the isomorphic substitution of Si with more ionic cations, in that in both cases the formation of strained units with 4-MR is favored by an increase in the ionicity of the T−O bond and hence in the framework flexibility.

A vibration around 500 cm^{-1} is shown to be characteristic of the D4R unit. This mode involves an in-phase breathing motion of the four-ring cage inside the D4R units with a contribution of motions external to the tetrahedra significantly increased with respect to the general trend observed in this frequency range. On the other hand, an antiphase breathing motion of opposite rings in the D4R unit is the main contribution to three vibrational modes in the 450−500 cm^{-1} region which show significant contributions of the guests and a hypsochromic shift in the as-made material compared to the calcined one. The shift is attributed to the change in the reduced mass of the mode due to the F^- participation and, in a lower amount, to the repulsion between the O atoms involved in the vibration and the closely confined fluoride anion. The localized character of these modes allow them to be used in general as a strong indication of the existence of F^- occluded into D4R units.[53]

In what concerns the vibrational behavior of the occluded TMI^+, the cation largely contributes to most modes, particularly in the framework soft mode frequency region (<500 cm^{-1}). The cation is remarkably confined in the direction perpendicular to the aromatic ring, giving rise to a decrease in the flexibility of the dihedral angles related to the rings with more than four members that cover the surface of the cavity containing the template. On the contrary, the SDA moves much more freely into roto-translations along the plane, featuring some temporary hydrogen-like interactions with the O atoms at the cavity surface. This brings about a host−guest interaction which involves polarization and/or charge transfer between both subsystems, as it is revealed by the analysis of the Born dynamic charges.

(55) Hong, S. B.; Lee, S.-H.; Shin, C. H.; Woo, A. J.; Alvarez, L. J.; Zicovich-Wilson, C. M.; Camblor, M. A. *J. Am. Chem. Soc.* **2004**, *126*, 13742−13751.
(56) Blasco, T.; Corma, A.; Díaz-Cabañas, M. J.; Rey, F.; Vidal-Moya, J. A.; Zicovich-Wilson, C. M. *J. Phys. Chem. B* **2002**, *106*, 2634−2642.

The overall picture derived from this work, mainly based on results obtained with theoretical techniques but strongly supported by experimental data, provides clear evidence that the structure-directing effect of charged organic cations together with occluded F^- ions involves not only the short-range repulsion characteristic of the cavity filling effect frequently invoked to explain structure-direction but also more complex interactions of electronic nature with the framework atoms. This issue deserves a thorough study of the electronic structure of Si-zeolites synthesized through the F-route which is out of the scope of the present work but will be the subject of a forthcoming paper.

Acknowledgment. The authors acknowledge support by SEP-FOMES2000 through Project "Cómputo Científico" for unlimited CPU time on the IBM-p690 32-processor supercomputer at UAEM and financial support by CONACYT(Mexico) (Project SEP05-46983) and the Spanish CICYT (Project MAT2006-033-56). Technical support from the CRYSTAL development staff is also gratefully acknowledged. F. Agulló-Rueda (ICMM-CSIC) is gratefully acknowledged for recording the Raman spectra. J.S.D.N. thanks CONACYT for a postdoctoral grant. Special thanks is deserved by Piero Ugliengo who has made available to us his useful collection of graphical tools.

Supporting Information Available: Additional information regarding the phase transition mode of the calcined ITQ-12, coupling between the framework and the TMI in the soft-mode region, and anaylsis of the Born atomic charges. Also fractional coordinate tables and Appendix. This material is available free of charge via the Internet at http://pubs.acs.org.

JA0730361